Life Sciences 235 (2019) 116859

Contents lists available at ScienceDirect

Life Sciences

journal homepage: www.elsevier.com/locate/lifescie

Unravelling the wound healing ability and mode of action of pyridine carboxamide oxime using *Caenorhabditis elegans* as potential prescreen wound model

Murugesan Pooranachithra[a], James Prabhanand Bhaskar[b], Deepa Murali[b], Shibendu Sekhar Das[b], Gnanasekaran JebaMercy[a], Venkateswaran Krishnan[b], Krishnaswamy Balamurugan[a,*]

[a] Department of Biotechnology, Science Campus, Alagappa University, Karaikudi 630 003, Tamil Nadu, India
[b] ITC Life Sciences & Technology Centre, Peenya Industrial Area, Phase 1, Bangalore 560058, Karnataka, India

ARTICLE INFO

Keywords:
C. elegans
Wound model
T. procumbens
New collagen synthesis
Pyridine carboxamide oxime
Chloromethyl nicotinamide and GSK-3

ABSTRACT

Aim: In the current scenario of ethical issues related to animal usage in research, the present study was intended to explore the proficient utility of nematode, *Caenorhabditis elegans* as wound model in preliminary screening of wound healing therapeutics.

Main methods: In this study, a new wounding protocol and quantitative assessment strategies for various healing parameters [survival, Reactive Oxygen Species (ROS), calcium signals, F-actin dynamics, new collagen synthesis and wound induced anti-microbial peptides] were developed and used for preliminary screening of wound healing actives from natural sources. Wound healing ability of positive lead *Tridax procumbens* (TP) and its major phytocompounds [Octa decenoic acid (ODA), Pyridine carboxamide oxime, known as Nicotinamide (NA) and Dimethyl Benz[*c*]acridine (DMB)] were assessed using *C. elegans* wound model and cell lines scratch wound healing assay. Mode of action of active lead was elucidated using metabolome analysis coupled with MALDI-MS followed by molecular docking.

Key findings: From the four tested methanolic extracts, TP was chosen as positive lead compared to control, Benzalkonium chloride (BKC) based on survival and new collagen synthesis analyses. Results indicated that the wound healing ability of TP was majorly contributed by NA. Further, it was found that NA acts in chloromethyl nicotinamide derivative form by interacting with the known wound healing biomarker, glycogen synthase kinase 3 (GSK-3) to exert wound healing ability.

Significance: The study evidenced that *C. elegans*, could be a reliable wound model for high-throughput screening of wound healing actives and to identify their possible mode of action.

1. Introduction

Wound healing is a process, in which reparation of damaged tissues and restoration of its function takes place. Various cell types are involved in effective wound healing to restore the tissue integrity. Though all biological systems have its automatic mechanism of repair, providing external support/stimuli can accelerate the process by inducing the tissue repair. The stimulant could be anything such as antiseptics, sulfa-antibiotics, skin barrier emollients, collagen specific enzymes, corticosteroids and any plant derivatives. According to Food and Drug Administration (FDA), the drug candidates targeting wound closure are very few and mostly composed of anti- inflammatory compounds (Silver sulfa diazene, Hibiclens, Thermazene, etc.,). An etiological research by Jiang et al reported that among wounded population in China, nearly 22.4% was treated with modern dressings or other novel technologies and remaining 77.6% of patients received only antibiotics

Abbreviations: AC, *Allium cepa*; BKC, benzalkonium chloride; CAMs, complementary and alternative medicines; CG, *Calotrophis gigantean*; CLSM, Confocal Laser Scanning Microscope; DCF-DA, DiChloroFluorescene-DiAcetate; DHB, Dihydroxybenzoic acid; DMB, 7,8-dimethyl Benz[*c*]acridine; FDA, Food and Drug Administration; GC–MS, Gas Chromatography-Mass Spectrometry; GSK-3, Glycogen synthase kinase 3; JC, *Jatropha curcus*; MALDI, Matrix Assisted Laser Desorption and Ionization; MS, Mass Spectrometry; MTT, 3-(4,5-dimethylthiazol-2-yl)-2,5-diphenyl tetrazolium bromide; NA, Pyridine-3-carboxamide, oxime, N/Nicotinamide; NGM, nematode growth medium; ODA, 9-Octa decenoic acid; PETA, People for the Ethical Treatment of Animals; q-PCR, Quantitative PCR; RMS, Root-Mean-Square deviation; ROS, Reactive Oxygen Species; RT, retention time; TP, *Tridax procumbens*

* Corresponding author.
E-mail address: bsuryar@yahoo.com (K. Balamurugan).

https://doi.org/10.1016/j.lfs.2019.116859
Received 19 July 2019; Received in revised form 23 August 2019; Accepted 8 September 2019
Available online 09 September 2019
0024-3205/

Table 1
List of primers used.

Gene name	Forward primer	Reverse primer
nlp-29	TGTTCTTGTCGTCCTTCTCG	ACTTTCCCCATCCTCCATAC
Itr-1	AAAGAAGGAATGCTCCGAGT	ACCAGTGCTTGCAAAAGTTC
col-19	CACACAAATGCTCCACCAAC	CTGGATTTCCCTTCTGTCCA

[1]. Moreover, still there is no direct drug candidate approved by FDA for healing by specifically targeting complete wound closure. Thus, development of drug candidates specific for wound closure is need of the hour for betterment of cutaneous wound care [2].

Natural compounds are the emerging sources of future drug candidates and there are numerous plant sources/plant derivatives which have been traditionally recognized to possess healing ability with therapeutic activities including antimicrobial/anti-inflammatory activity, better tissue remodeling ability and activation of immune & migrating cells [3]. Moreover, there are number of formulations comprising of plant extracts and their combinations have been patented for its antibiotic, anti-inflammatory and wound healing activity [4–6]. This evidences that isolation and identification of phytochemicals specific to a particular healing property and their combinatorial ability is a prudent way of approach for future therapeutics. Accordingly, plants derived compounds are gaining great attention as Complementary and Alternative Medicines (CAMs) for their wound healing activity [7,8].

In this regard, numerous animal models are being used by the researchers for screening and identification of active drug candidates for wound healing [9–11]. Since the use of animals is often debated and numbers of animal usage is limited [12], development of methods that are actually relevant to human health is required to reduce the extensive use of animals (People for the Ethical Treatment of Animals (PETA) organization). In this context, multiple non animal models (*Artemia salina*, *C. elegans*, *Drosophila melanogaster,* etc.,) are being employed in various fields of research including wound investigations [13,14]. In concatenation with the aforesaid, 60–80% of genome and nearly 83% of proteome of *C. elegans* were found to be orthologous to that of human system [15,16]. Moreover, counterparts of 65% of disease causing genes were also reported to be present in *C. elegans* [17]. Owing to this evolutionary conservation, *C. elegans* is emerging as a valuable model in various fields of research including neuroscience, development, signal transduction, cell death and RNA interference, aging, biomedical and environmental toxicology as well as wound research [18].

Notable findings using *C. elegans* as wound model include the discovery of function and active mechanism of several major signaling molecules such as ROS and calcium signals during repair and regeneration [19,20] which are found to be the underlying signaling molecules for wound repair in humans as well. This evidences that the results obtained from this nematode model could be translated to higher mammals. Further, the *C. elegans* wound models have also supported in identification of new insights into wound repair. For instance, function of death associated protein kinase 1 (DAPK1) in regulating apoptosis and autophagy is known [22,23] whereas its additional function in negatively regulating the process of wound repair was identified using *C. elegans* wound model [21]. Furthermore, the preliminary high throughput screening of probable drug candidates for wound healing become easy with *C. elegans* than other animal models due to the simple and expedite procedure of preparing umpteen wounded worms at a single stretch. Hence, the present study aims to uncover the utility of a non-animal model, *C. elegans* as wound model for preliminary screening of potential therapeutics with wound healing ability.

2. Materials and methods

2.1. Maintenance of C. elegans

The wild type strain (Bristol N2) and transgenic lines of *C. elegans* (CZ14748, HBR4 and TP12) were obtained from *Caenorhabditis* Genetics Center, University of Minnesota, USA. As per the standard protocol, the wild type and transgenic worms were maintained routinely on nematode growth medium (NGM) agar plates seeded with a lawn of *Escherichia coli* OP50 (An uracil auxotroph, which is used as the food source for *C. elegans*) at 20 °C and 15 °C, respectively [24]. For experiments, the age synchronized young adult stage of nematodes was obtained by lysing the gravid hermaphrodites with an alkaline sodium hypochlorite solution containing 5 M potassium hydroxide (KOH) in the ratio of 1:1. For all assays, worms were used in triplicates [25].

2.2. Glass wool mediated wounding of voluminous C. elegans

Till date, femtosecond laser and microinjection needles were used to injure single *C. elegans* at a time [26] and micrometer-scale fine glass shards [27] for more number of wound populations. Inspired by the wound practice described by Zhang et al. [27], a new protocol was developed to obtain more number of wounded worms at a stretch using truncated glass wool pieces. Around 50 mg of autoclaved truncated glass wool pieces were used to injure the worms in their young adult stage by vortexing for 1 min. The worms were then washed gently with M9 buffer and visualized under stereo microscope (Nikon SMZ1000, Japan) to identify the occurrence of injury.

2.3. Localization of site of injury

Nile red, a chromogenic dye was used for localization of site of glass wool mediated injury in worms under bright field microscope. A 5 μL of Nile red (RM9734, Himedia) from 1 mg/mL stock solution was added to the glass wool and tapped few times for allowing the dye to mix with the glass pieces. Young adult stage of worms was transferred to the tube and vortexed for a minute. A gentle wash with M9 buffer was given to settle down the glass pieces leaving behind the wounded worms in the supernatant. After, the worms were imaged using bright field microscope (Nikon SMZ1000, Japan) for localization of the site of injury at different magnifications.

2.4. Electron paramagnetic resonance (EPR) spectroscopy

Equal numbers of wounded worms and unwounded control worms were homogenized in 15% of glycerol and EPR measurements were acquired immediately on Bruker EMX Plus instrument with slight modifications [28]. All measurements were done at microwave Frequency of 9.769182 GHz, 3480.00 centre field, 2000 G sweep width and 2.0×10^3 receiver gain. The continuous-wave (CW) EPR spectra were obtained with a modulation frequency of 100 kHz, modulation amplitude of 4.0 G and 10 mw power at room temperature for 20 scans.

2.5. Fourier-transform infrared (FTIR) spectroscopy

Equal numbers of wounded worms and unwounded control worms were ground with 100 mg of potassium bromide and dried under vacuum to prepare a pellet. Infrared spectra were then collected in the range of 400 to 4000 cm^{-1} using an FTIR spectrometer (Bruker Tensor 27) and the values were plotted as intensity against wavenumber as described earlier [29].

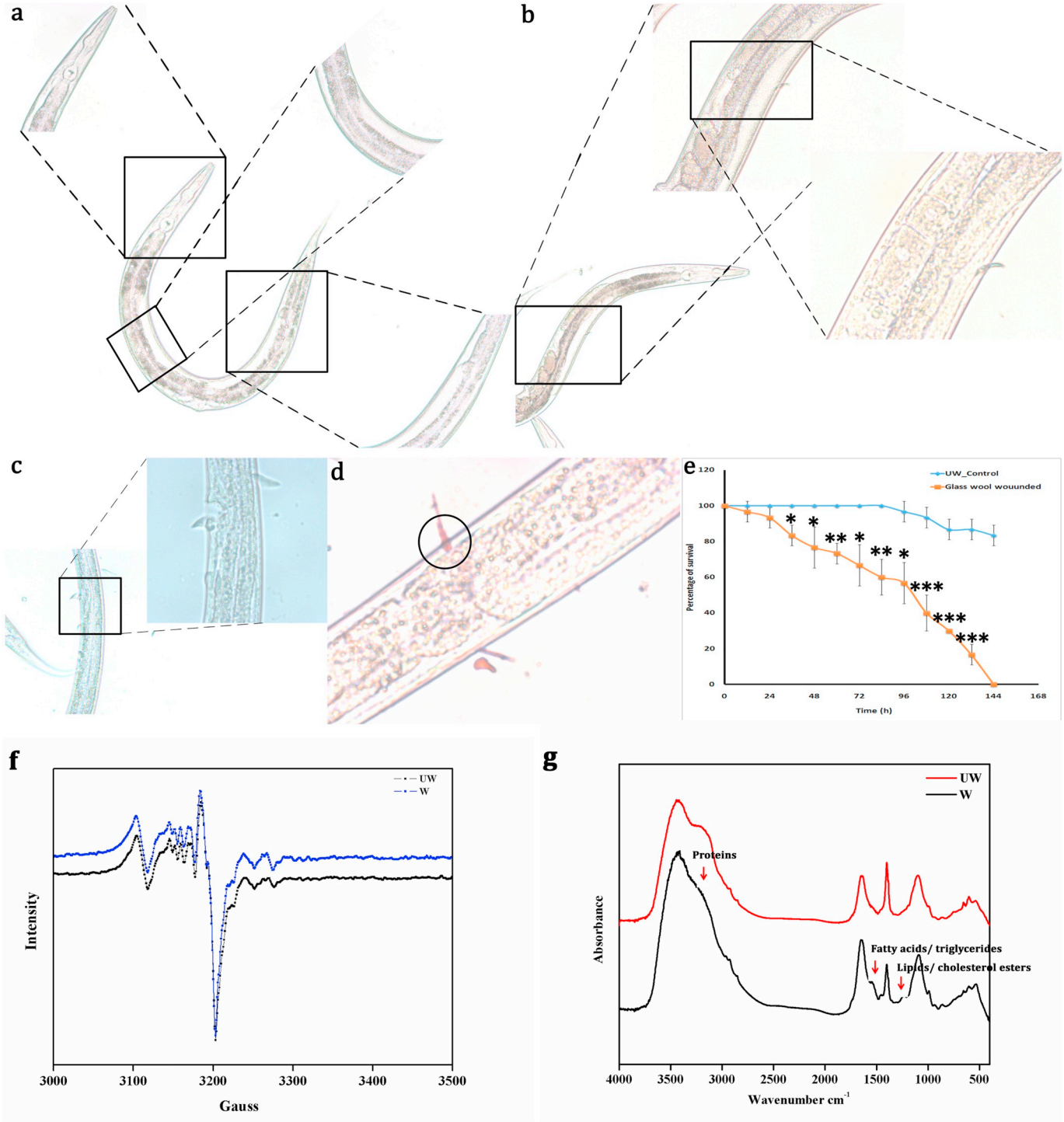

Fig. 1. Wounding of *C. elegans* by glass wool mediated injury (a) Control unwounded worm with intact muscles and epidermis (b) Glass wool wounded worm with the wounded region, indicated with an arrow mark (The glass piece is found to be inserted from the epidermal outer skin to the inner muscle layer) (c) Glass wool wounded worm with the incision created by the glass piece (d) localization of site of injury using Nile Red. (e) Impact of glass wool mediated injury on survival of worms. The experiment was performed independently for three times and the differences among the repetitions were given in terms of standard deviation. Statistical analysis was performed using two tailed Students *t*-Test. (f) EPR spectra of wounded and unwounded worms (g) FT-IR spectra of wounded and unwounded worms (* - $p < 0.05$; ** - $p < 0.01$; *** - $p < 0.005$). (For interpretation of the references to colour in this figure legend, the reader is referred to the web version of this article.)

2.6. Survival analysis

Analysis was performed in 24 well plates with a total of 500 µL reaction volume. Optimum concentration of test methanolic extracts/ derivatives were identified by incubating the worms with extracts/ derivatives at various concentrations (50–250 µg/mL) and assessing their viability. Concentration, at which number of worms was comparable to untreated worms, was taken as optimum concentration. Later, test actives were applied to wounded worms with untreated wound control and survival was monitored till the control becomes

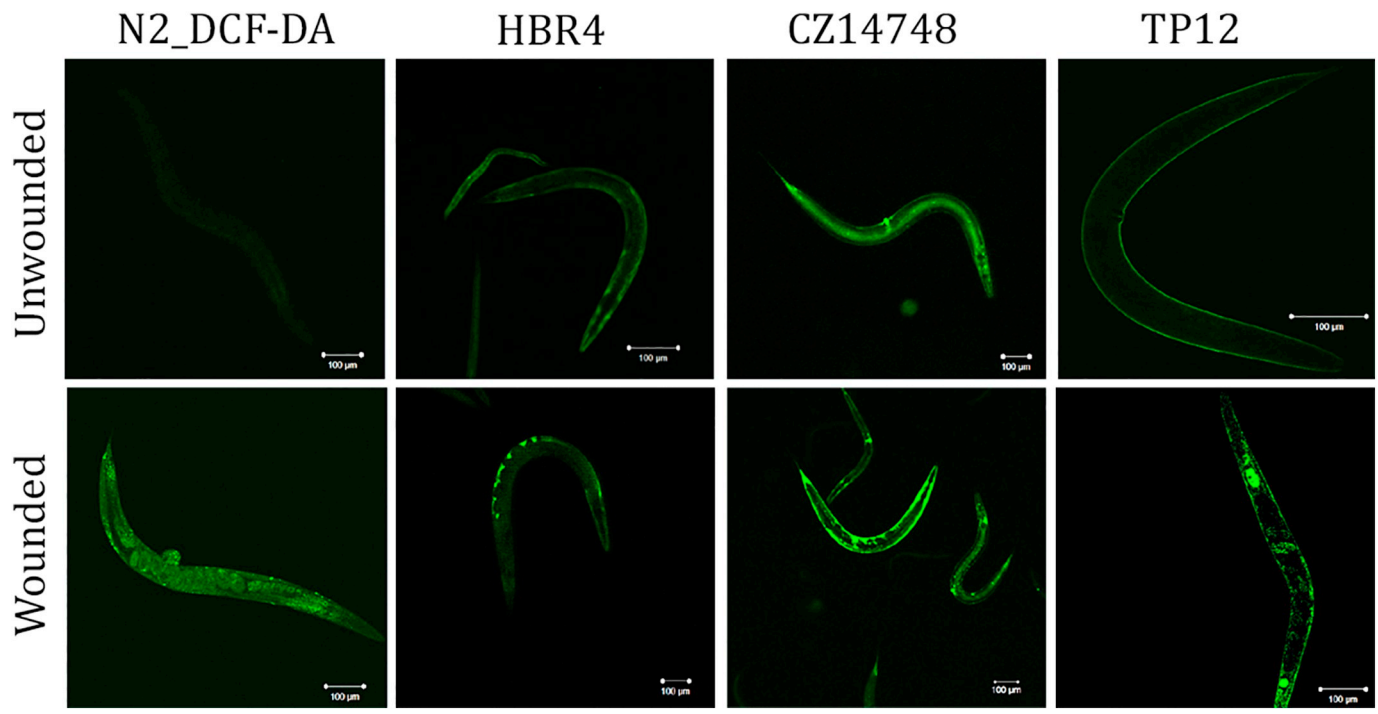

Fig. 2. Assessment of healing parameters after glass wool mediated injury. (Pictures from left to right indicate the results of ROS, calcium signals, F-actin dynamics and new collagen synthesis).

zero. A known active principle [30], BKC was taken as control for the study.

2.7. Measurement of extracellular Reactive Oxygen Species (ROS)

The level of ROS was assessed using DiChloroFluorescene-DiAcetate (DCF-DA) (D6883, Sigma), a fluorescent indicator as described by Durai et al. [31] and subsequently documented using Confocal Laser Scanning Microscope (CLSM) (Carl Zeiss, Germany).

2.8. Microscopic imaging of transgenic worms

To examine the calcium flux, F-actin dynamics and collagen, transgenic line of *C. elegans* named HBR4, CZ14748 and TP12 respectively were utilized [20,32]. Wound investigations were performed in the aforementioned strains and imaged using CLSM.

2.9. Collagen estimation

Quantification of new collagen synthesis in *C. elegans* was performed as described using Sircol™ Soluble Collagen Assay kit [32]. Results were depicted in bar charts for absorbance of Sircol dye bound to the newly synthesized collagen in the test samples.

2.10. Quantitative PCR (q-PCR) analysis

RNA was isolated using TRIzol™ reagent (RNA X Press reagent, Himedia) and was then reverse transcribed using oligo dT primer and MultiScribe™ Reverse Transcriptase (Applied Biosystems) enzyme as per the manufacturer's guidelines. q-PCR analysis was carried [33] out in triplicates to analyze the expression pattern of candidate genes using gene-specific primers, designed using Primer3 (*v*. 0.4.0) online tool (Table 1).

2.11. Gas chromatography-mass spectrometry (GC–MS)

GC–MS analysis was performed using Agilent GC7890A/MS5975C instrument encompassing Agilent DB5MS capillary column. Methanolic extract of TP was injected in to the column and the phytocompounds were identified using NIST library based on their mass and retention time (RT).

2.12. Scratch wound healing assay in Hep3B (human hepatoma) cells

MTT assay and scratch wound healing assay was performed as described by Premarathna et al. 2019 [34]. Scratch wound closure was visualized and imaged using an inverted microscope (Nikon eclipse Ti, Inverted fluorescent microscope). Images were analyzed by Image Pro software by monitoring the width of the scratch area at different time intervals (0, 6 and 24 h) to calculate rate of cell migration and wound closure.

2.13. Metabolite analysis

Test active was applied at optimum concentration to single worm and incubated at 20 °C to allow for healing. Later at 12& 24 h of treatment, exometabolome were separately collected in new sterile tubes. Endometabolome (single worm) was sonicated in acetonitrile and vacuum dried with equal volume of 60% of acetonitrile and dissolved in 5 µL of 0.1% trifluoroacetic acid in 60% of acetonitrile. Exometabolome was directly vacuum dried and dissolved as described earlier. Next to that, endometabolome as well as exometabolome were spotted with Dihydroxybenzoic acid (DHB) matrix and analyzed for metabolites using MALDI-MS (Axima performance mass spectrometer) with positive ionization mode and linear detector [35]. The acquired spectra was manually annotated and analyzed for their derivatives.

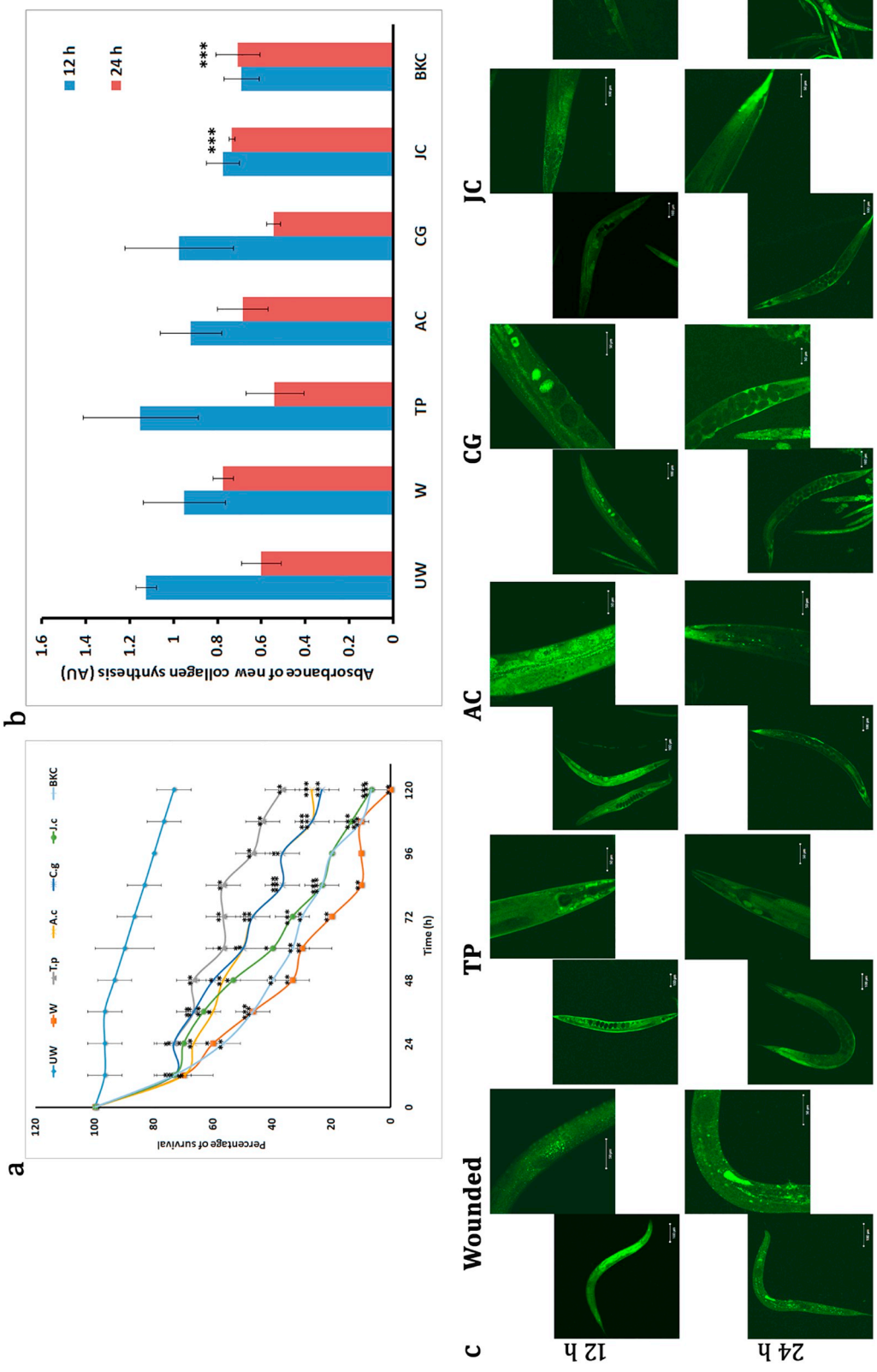

Fig. 3. Screening of phyto therapeutics for wound healing using *C. elegans* wound model (a) survival based screening (b) estimation of new collagen synthesis of test extracts after 12 and 24 h of treatment (c) microscopic imaging of new collagen synthesis based screening using TP12. Statistical analysis was performed using two tailed Students *t*-Test. (* - $p < 0.05$; ** - $p < 0.01$; *** - $p < 0.005$).

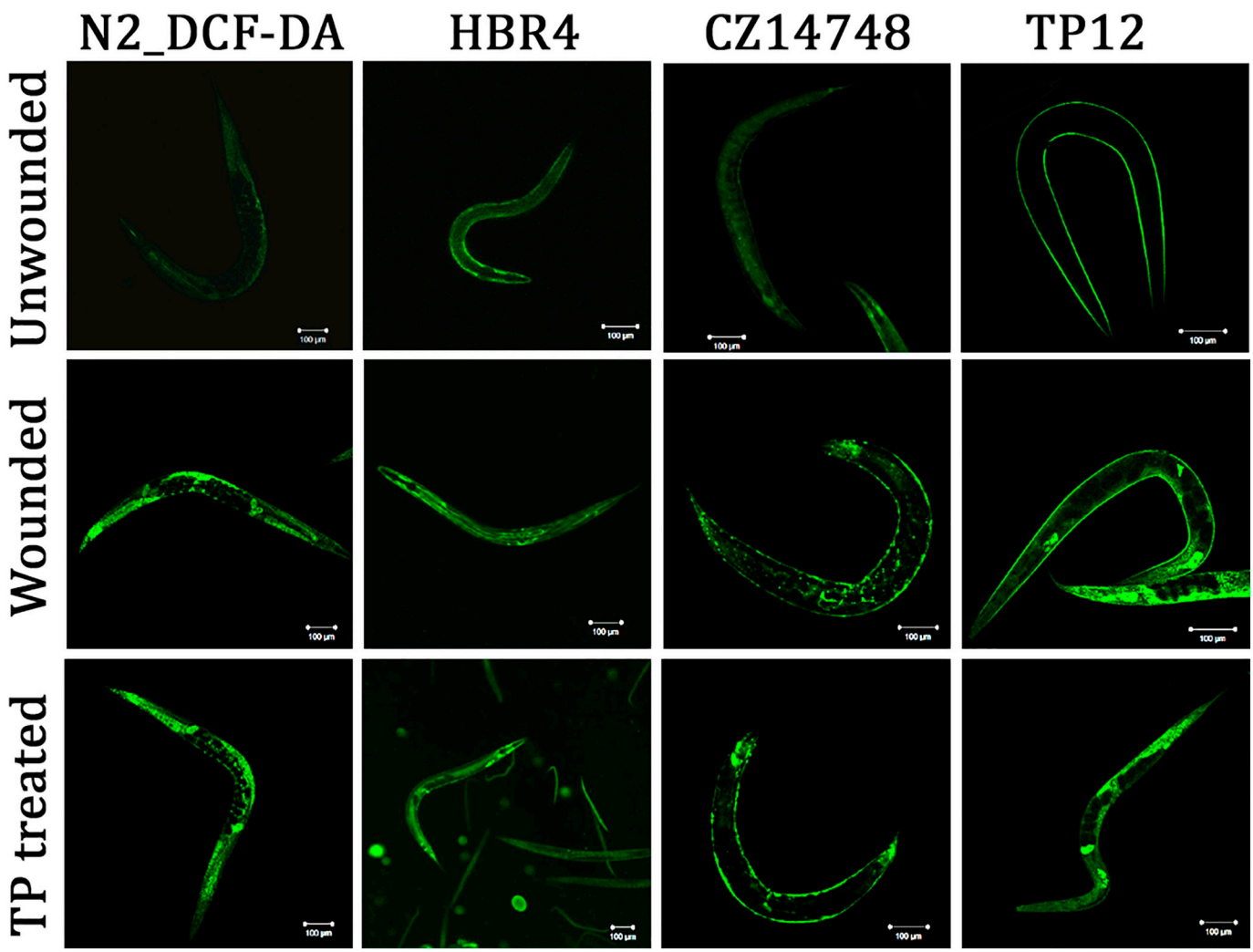

Fig. 4. Assessment of healing ability of screened phyto active (TP) after 12 h of treatment. (Pictures from left to right indicate the results of ROS, calcium signals, F-actin dynamics and new collagen synthesis).

2.14. Bioinformatics analysis

Molecular docking of each ligand molecule was performed by docking it with a wound healing biomarker, GSK-3 to assess their mode of healing [36]. The 3D conformation of each ligand molecule structures was obtained in sdf format from PubChem database and converted to MOL2 format by molecule file format conversion via ChemAxon JChem with Convert - UNM Biocomputing online application. The 3D crystal structure of GSK-3β from human origin (1H8F) was obtained from Protein Data Bank (PDB). The 3D crystal structure of GSK-3 ortholog of human GSK3A and GSK3B in *C. elegans* is unavailable. Hence, its 3D structure was predicted using SWISS-MODEL, online server for protein structure homology modeling and structure confirmation was insured by analyzing the aminoacid residues on Ramachandran plot. Later, each ligand molecule was docked individually with GSK-3 of both *C. elegans* origin as well as human origin and binding energies were predicted using SWISS-DOCK (a free online docking server) where binding modes were scored using their full fitness and ranked based on average full fitness of the elements [37].

2.15. Statistical analysis

All experiments were performed independently in triplicates. Results are presented as mean ± standard errors of the mean (SEM). The significance of statistical difference was analyzed using unpaired *t*-test. The statistical significance of $p < 0.05$ (represented with *); $p < 0.01$ (represented with **); $p < 0.005$ (represented with ***) was considered for this study.

3. Results

3.1. Glass wool produces injuries on C. elegans

Wounding of voluminous worms in the presence of glass wool was found to puncture the outer layer of the worm ranging from outer most dermis to the inner most muscles (Fig. 1b,c), unlike unwounded control (Fig. 1a) wherein the outer layer remains intact from head to tail. Washing the worms with M9 buffer after injury was found to remove the perforated glass piece in *C. elegans*. Application of Nile red with glass piece prior to wound practice supported the localization of site of injury as well as evidenced the occurrence of injury on *C. elegans* (Fig. 1d). Survival analysis on glass wool wounded worms denoted reduction in survival after injury. A 50% and 100% of mortality of wounded worms was observed at 96 h and 144 h, respectively (Fig. 1e). EPR spectra (Fig. 1f) indicate the alterations in the free radicals after injury. FT-IR spectra (Fig. 1g) also indicate the alterations in the outer skin layer composition notably in lipids/cholesterol esters ($1456\ cm^{-1}$), fatty acids/triglycerides ($1744\ cm^{-1}$) and proteins ($3280\ cm^{-1}$).

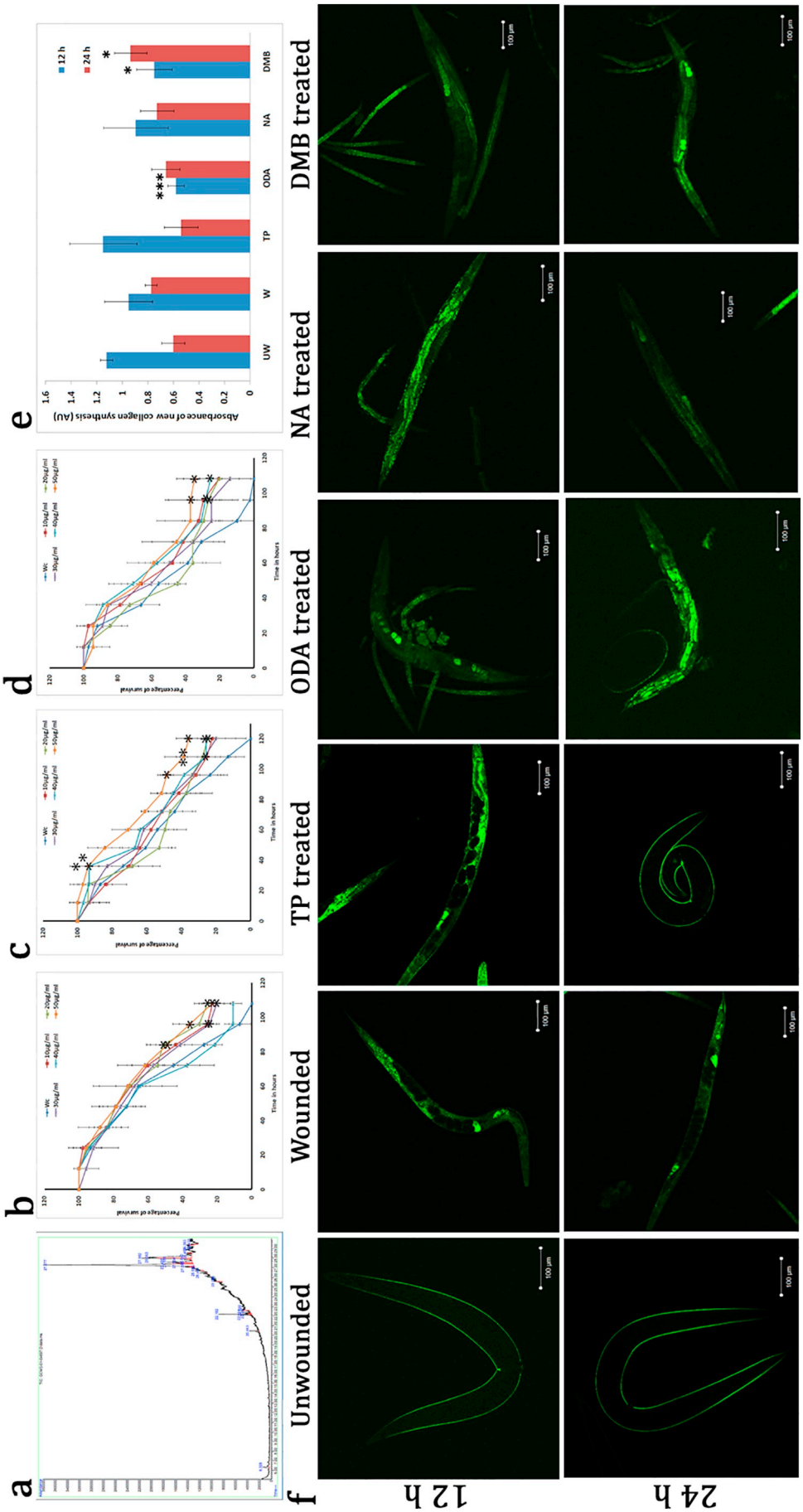

Fig. 5. Identification and assessment of healing ability major phytocompounds of screened phyto active (TP). (a) GCMS/MS chromatogram of TP (b) survival based wound healing assessment of ODA (c) survival based wound healing assessment of NA (d) survival based wound healing assessment of DMB (e) estimation of new collagen synthesis of TP and its major phytocompounds after 12 and 24 h of treatment (f) microscopic evaluation of new collagen synthesis after 12 and 24 h of treatment. Statistical analysis was performed using two tailed Students t-Test. (* - $p < 0.05$; ** - $p < 0.01$; *** - $p < 0.005$).

Table 2
List of phytocompounds identified by GCMS/MS (High).

Peak No.	RT (Min)	Name of the identified compound	Peak area in %
1.	27.277	9-Octadecenoic acid	43.89
2.	28.063	Pyridine-3-carboxamide, oxime, N (Nicotnamide)	14.41
3.	27.982	Benz[c]acridine, 7,8-dimethyl-	12.29
4.	27.585	Cyclohexane, 1-(1,5-dimethylhexy	6.69
5.	27.405	2-Octadecyl-propane-1,3-diol	3.03
6.	27.504	Pyridine-3-carboxamide, oxime, N	2.76
7.	22.182	11-Octadecenoic acid, methyl ester	2.58
8.	26.682	Heptadecanal	1.77
9.	27.090	Pyridine-3-carboxamide, oxime, N	1.64
10.	6.328	Ethylbenzene	1.56
11.	25.586	Pyridine-3-carboxamide, oxime, N	1.26
12.	26.461	Pyridine-3-carboxamide, oxime, N.	1.21
13.	22.584	14-Methyl-8-hexadecyn-1-ol	0.97
14.	22.124	9,17-Octadecadienal	0.97
15.	20.463	Hexadecanoic acid, methyl ester	0.93
16.	22.287	2-Dodecen-1-yl(−)succinic anhydride	0.88
17.	29.433	Pyridine-3-carboxamide, oxime, N	0.87
18.	29.363	Pyridine-3-carboxamide, oxime, N	0.80
19.	28.489	Propiophenone, 2′-(trimethylsilo	0.78
20.	27.842	erythro-9,10-Dibromopentacosane	0.72

3.2. Assessment of healing parameters upon injury

Healing parameters including ROS, calcium signals, F-actin dynamics and new collagen synthesis were assessed after injury at 12 h on *C. elegans* using DCF-DA staining, HBR4, CZ14748 and TP12 respectively. Results indicated the increased level of ROS, elevated calcium signals specifically at the wounded site, induced F-actin and new collagen synthesis distinctively at the site of injury (Fig. 2).

3.3. Screening of test extracts for wound healing ability

Optimum concentration of four test methanolic extracts [TP, *Allium cepa* (AC), *Calotrophis gigantea* (CG) and *Jatropha curcus* (JC)] and BKC was identified to be 50 µg/mL, 50 µg/mL, 50 µg/mL, 100 µg/mL and 10 µg/mL respectively (Data not shown). Optimum concentration of each test active was subjected for evaluation of their healing ability on wounded worms by survival analysis. Results indicated that the survival of wounded worms upon TP treatment was 40% which was followed by control was (10%) and untreated wounded control (0%) (Fig. 3a). Based on the survival improvement in wounded worms, healing ability of the test actives is as follows: TP > AC > CG > JC = BKC. Later, the test actives were subjected to screening based on synthesis of new collagen. In this regard, estimation of new collagen synthesis was done at 12 and 24 h of treatment using Sircol™ Soluble Collagen Assay kit. The results indicated, increase in new collagen synthesis in all the test extracts than the control BKC (Fig. 3b) and the order of healing based on new collagen synthesis, is as follows: TP > CG > AC > JC > BKC. Further, the new collagen synthesis induced by the test actives were confirmed through imaging using an engineered strain col-19::GFP (TP12), a transgenic *C. elegans* model. Results of microscopic analysis after 12 and 24 h of treatment with test actives (Fig. 3c) also indicated the improved new collagen synthesis by TP extract.

3.4. Assessment of healing parameters after treatment with the active lead

Healing parameters such as ROS, calcium signals, F-actin dynamics and new collagen synthesis were assessed after injury at 12 h of treatment in the presence of screened active (TP) with wounded and unwounded control. Results indicated increase in all tested healing parameters in treated than wounded control (Fig. 4).

3.5. Identification and assessment of healing ability of phytoactives

Chromatogram obtained from GC–MS analysis of TP extract (Fig. 5a) resulted in 20 contributing phytocompounds as listed in Table 2 where octa decenoic acid (ODA) was the major compound based on the area covered by the compound (43.89%). The second major compound was Pyridine-3-carboxamide, oxime, N (14.41%) commonly known as Nicotinamide (NA). Third major compound was dimethyl benzacridine (DMB) which covers 12.29% of area. Healing ability of identified major phytocompounds in varying concentrations (10–50 µg/mL) was assessed through survival analysis. Results indicated an improved survival was seen in all tested concentrations with maximum survival of 25% at 20 µg/mL of ODA (Fig. 5b), 35% at 50 µg/mL of NA (Fig. 5c) and 34% at 50 µg/mL of DMB (Fig. 5d). Later, new collagen synthesis was analyzed at 12 and 24 h through estimation (Fig. 5e) and microscopic imaging (Fig. 5f) and the results indicated an induced collagen synthesis at 12 h in all test actives which was reduced to baseline pattern as observed in unwounded control upon treatment with TP and NA (Fig. 5e&f).

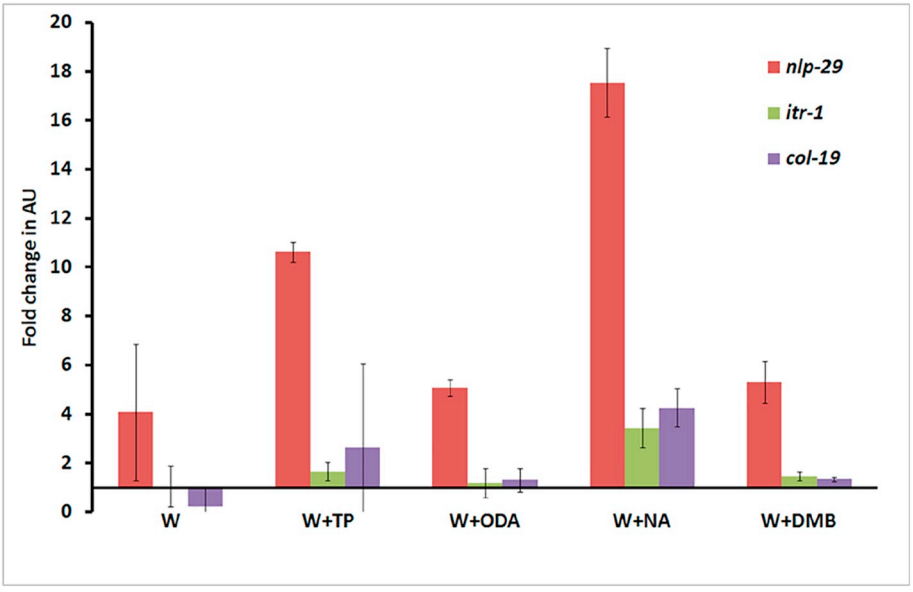

Fig. 6. q-PCR analysis based molecular assessment of healing ability of TP and its major phytocompounds.

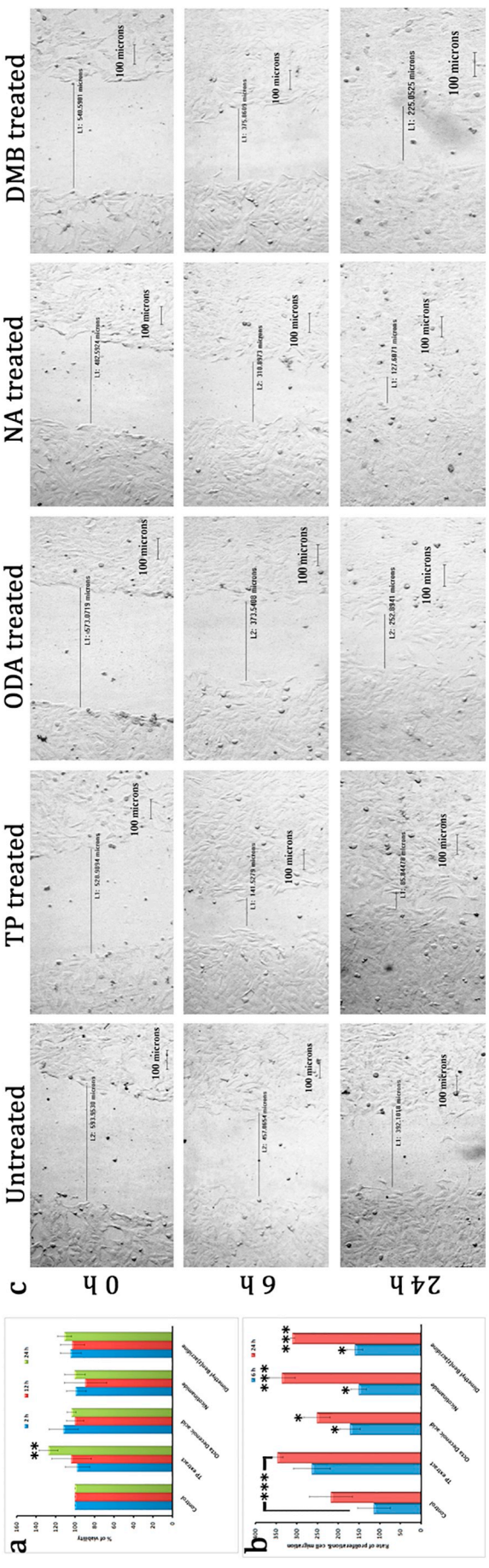

Fig. 7. Cell line based assessment of healing ability of TP and its major phytocompounds. (a) cytotoxcity analysis (b) assessment of rate of proliferation and cell migration (c) microscopic evaluation of healing ability.

3.6. Molecular assessment of healing ability of photo actives

q-PCR analysis of candidate genes such as *nlp-29*, *itr-1* and *col-19* was performed after 12 h of treatment. Results indicated an increase in fold change of all candidate genes during treatment with TP, ODA, NA and DMB when compared to wounded control (Fig. 6). Based on the fold change, order of healing ability of test actives is as follows: NA > TP > DMB > ODA.

3.7. Cell lines based assessment of healing ability of phyto actives

Scratch wound healing assay was performed in Hep3B cells to evaluate the healing ability of the test phyto actives after assessing their toxicity by cell viability study at 2, 12 and 24 h (Fig. 7a). Results of cell viability study indicated the non-toxic nature of the test actives. Scratch wound healing assay results clearly denoted the closure ability of the test actives when compared to untreated control. Wound diameter at 0, 6 and 24 h were identified by microscopic imaging of cells and the results indicated that the wound was nearly closed at 24 h upon treatment with TP and NA respectively (Fig. 7c). From the wound diameter at different time points, rate of proliferation and migration was calculated for each test phyto actives where it was apparent that all the test actives showed an increase in cell proliferation and migration (Fig. 7b). Based on the rate of proliferation and migration order of test phyto actives are as follows: NA > TP > DMB > ODA.

3.8. Mode of healing of NA

Metabolome analysis of single worm was performed to identify the mode of healing of NA after treatment for 12 and 24 h. Results indicated the presence of masses of 18 and 31 differentially appeared metabolites specifically in wounded worm treated with NA at 12 and 24 h respectively. Metabolites of NA respective to the identified mass from MALDI-MS were spotted using Pubchem and listed in Tables 3 & 4. Among the identified metabolites, a metabolite with the mass of 170 was constantly found in all three replicates at 24 h, which was found to be chloromethyl nicotinamide (Fig. 8a). As the identified metabolite of nicotinamide exists in three structural variants such as 2-Chloro-*N*-methylnicotinamide, 6-Chloro-*N*-methylnicotinamide and 3-Pyridinecarboxamide, N-(chloromethyl)-) (Fig. 8b), elucidation of mode of action of NA was performed using all the three variants by molecular docking with a known wound healing biomarker, GSK-3 of *C. elegans* and humans as target receptor. Since, protein crystal structure of GSK-3 for *C. elegans* is unavailable it was predicted using SWISS-MODEL. The modeled structure was assessed to be structurally similar to GSK-3 of human origin (1H8F) with RMS value of 0.609 while superimpose them together (Fig. 9a) and validated through Ramachandran plot analysis where most of the residues were fallen in the favorable region with 95.68% (Fig. 9b). Molecular docking of the structural variants of identified metabolite with GSK-3 of *C. elegans* (Modeled through SWISS-MODEL) and humans (1H8F) revealed the active binding of all the three structural variants with GSK-3 of *C. elegans* (Fig. 9c) as well as human (Fig. 9d) with a lower binding energy of around −6.00 to −6.60 as tabulated in Table 5.

4. Discussion

Nowadays, usage of animal models in research is limited due to highly stringent regulations, concerned to ethical issues. This triggers the necessity of finding an alternate to animal models in biological research, which could provide versatile virtues relevant to the human health. In this regard, *C. elegans* affords ample promising prospects to act as an efficient alternate animal model in diverse fields of science including wound research, as the skin architecture of this elegant miniature model is simple and comparable to higher eukaryotes [38]. Some of the techniques accustomed to the instigation of injuries in *C.*

Table 3
List of masses differentially identified in wounded worm after 12 h of NA treatment.

S. No.	Mass identified	Name of compound	PubChem ID
1.	124.119	[14C]-Nicotinamide	644257
2.	219.288	N-Azepan-1-yl-nicotinamide	12499584
3.	219.288	(4-(Aminomethyl)piperidin-1-yl)(pyridin-3-yl)methanone	28706808
4.	219.187	Pyridinium, 1-methyl-3-[[(2,2,2-trifluoroethyl) amino] carbonyl]-	71343174
5.	158.585	Nicotinamide hydrochloride	91408
6.	158.108	2,4-Difluoronicotinamide	67369421
7.	139.172	Thionicotinic acid	571572
8.	139.129	3-(alpha-Fluoroacetyl)pyridine	19023729
9.	192.262	N-(3-Methylbutyl)pyridine-3-carboxamide	836813
10.	192.262	N-Pentylpyridine-3-carboxamide	1733355
11.	192.262	N-Tert-Butyl-*N*-methylnicotinamide	19976415
12.	192.262	N,N-Diethyl-4-methylpyridine-3-carboxamide	58607459
13.	192.262	N-Butyl-*N*-methylpyridine-3-carboxamide	71344355
14.	214.693	1-Tert-Butyl-3-carbamoylpyridin-1-ium chloride	12791790
15.	132.122	3H-Pyrrolo[3,4-*c*]pyridin-3-one	53439661
16.	354.963	Pyridinium, 3-carbamoyl-1-tetradecyl-, chloride	3048435
17.	370.999	Dichlorodi(nicotinamide)iron	83015
18.	374.087	Cobalt, dichlorobis(nicotinamide)-	25547

elegans for wound infection with *D. coniospora* [39], micro-injection needle, femtosecond laser treatment [26] and micrometer-scale fine glass shards [27] to create injury. The aforementioned techniques could create only an injury per worm at a time or infection mediated while obtaining more number of wounded worms. Nevertheless, this study aims to develop a new wounding protocol, which could provide voluminous wounded worms at a single stretch and support preliminary screening of wound healing therapeutics from natural sources.

Wound protocol was established in *C. elegans* and confirmed through microscopic imaging, survival, FT-IR and EPR analysis (Fig. 1). Further, the established wound model was subjected to preliminary screening based on survival and new collagen synthesis assays, which resulted in the identification of an active lead, TP with maximum healing ability when compared to others (Fig. 3). Further, various healing parameters were assessed upon treatment with TP wherein, elevated level of ROS, calcium signals, F-actin dynamics and new collagen synthesis was observed (Fig. 4). Elevated level of ROS during TP treatment indicates the activation of innate immune signaling and improved wound repair action as reported earlier [19,40]. In addition, increase in Ca^{2+} signals upon TP treatment specifies its role in enhancing the closure machinery, which is in correspondence with the previous report wherein, the exclusive role of Ca^{2+} signals in entailing the repair process is well described [20,41]. Similarly, in accordance with the earlier reports [42,43], escalation of F-actin dynamics and new collagen synthesis in the presence of TP signifies the increased integrity and enhanced remodeling, respectively.

Table 4
List of masses differentially identified in wounded worm after 24 h of NA treatment.

S. No.	Mass identified	Name of compound	PubChem ID
1.	125.102	2-Fluoro-3-formylpyridine	11434944
2.	125.102	2-Fluoro-5-formylpyridine	16414246
3.	125.102	3-Pyridinecarbonyl fluoride	53847896
4.	170.596	3-Pyridinecarboxamide, N-(chloromethyl)-	151307
5.	170.596	2-Chloro-*N*-methylnicotinamide	12286955
6.	170.596	6-Chloro-*N*-methylnicotinamide	12364230
7.	180.163	Hydroxylamine, *O*-acetyl-N-nicotinoyl-	150292
8.	180.187	1-(2-Amino-2-oxoethyl)pyridin-1-ium-3-carboxamide	422137
9.	180.207	N-Propan-2-yloxypyridine-3-carboxamide	3028391
10.	216.133	(Nicotinamidomethyl)phosphonic acid	274553
11.	220.228	N-(3-Oxopentanoyl)pyridine-3-carboxamide	12820673
12.	229.283	N-[(*E*)-Cyclohex-3-en-1-ylmethylideneamino]pyridine-3-carboxamide	5339510
13.	411.177	5-(Tributylstannyl)nicotinamide	22420973
14.	140.142	Pyridine-3-carboxamide hydrate	16638467
15.	140.117	4-Fluoropyridine-3-carboxamide	45079851
16.	140.117	5-Fluoronicotinamide	101264
17.	140.117	2-Fluoronicotinamide	252367
18.	140.117	6-Fluoronicotinamide	348575
19.	188.611	Formohydroxamic acid, *O*-methyl-1-(3-pyridyl)-, hydrochloride	3063922
20.	188.23	N-(Buta-2,3-dien-1-yl)-*N*-methylpyridine-3-carboxamide	71445660
21.	188.23	N-(1,1-Dimethylprop-2-ynyl)-3-pyridylcarboxamide	729751
22.	202.257	N,N-Diallylnicotinamide	4152740
23.	202.638	3-Carbamoyl-1-(2-hydroxyethyl)pyridinium chloride	2835577
24.	312.706	Pyridinium, 3-(aminocarbonyl)-1-(phenylmethyl)-, perchlorate	10913984
25.	312.882	3-Carbamoyl-1-undecylpyridinium chloride	200560
26.	321.785	1-[3-(3-Carbamoylpyridin-1-ium-1-yl)propyl]pyridin-1-ium-3-carboxamide chloride	356719
27.	191.234	Piperazin-1-yl(pyridin-3-yl)methanone	770194
28.	191.234	N-[(*Z*)-Butan-2-ylideneamino]pyridine-3-carboxamide	5399343
29.	191.234	Isobutyraldehyde nicotinoyl hydrazone	9574224
30.	309.989	Pyridinium, 1-(2-bromoethyl)-3-carbamoyl-, bromide	3048432

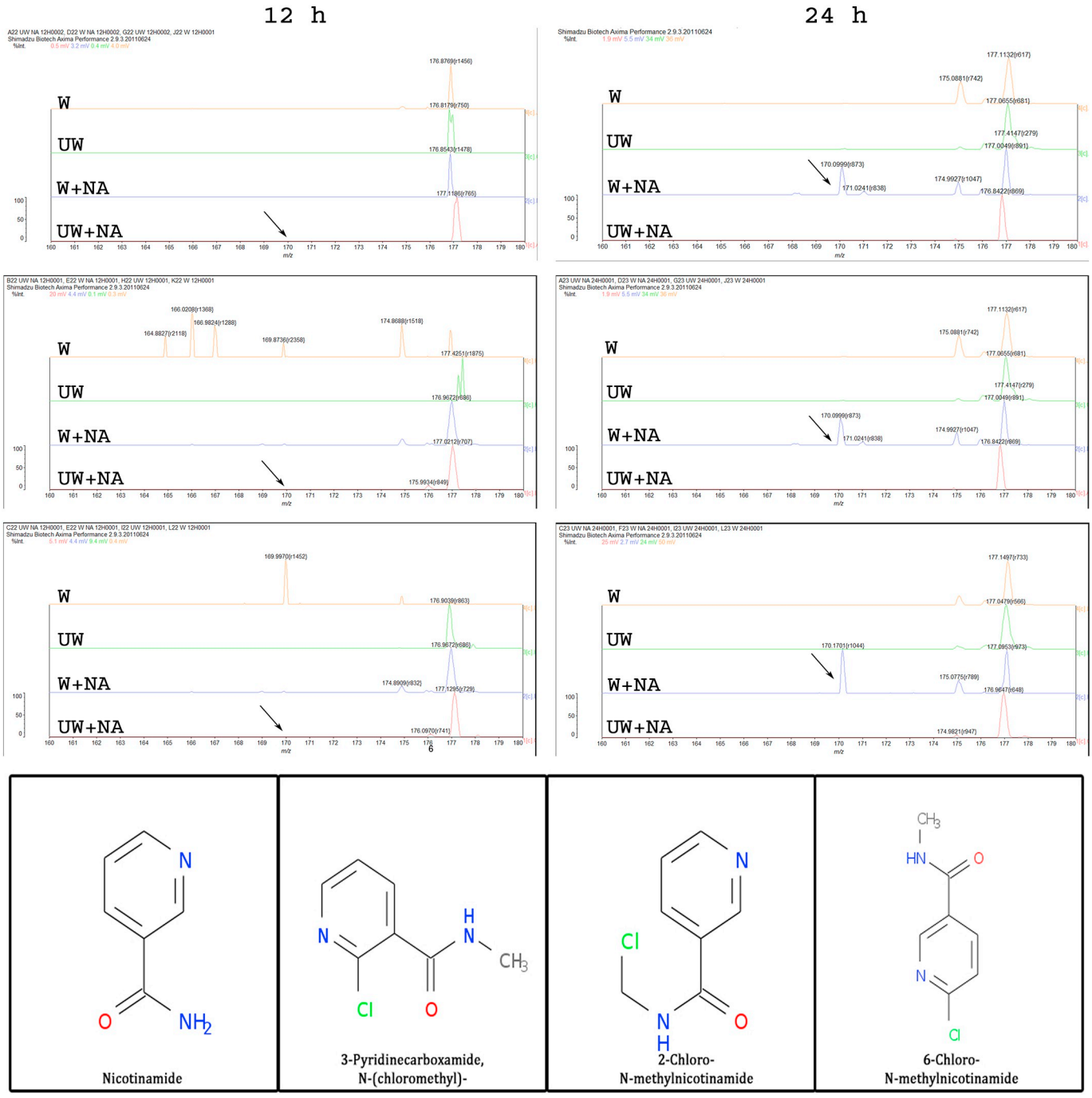

Fig. 8. Metabolome analysis of wounded worm treated with NA. (a) Mass Spectrum obtained from MALDI at 12 and 24 h from wounded, unwounded and treated worms respectively (b) different structural variants of identified active metabolite of NA (chloro methyl nicotinamide).

Furthermore, phytocomposition of TP was analyzed by GC–MS analysis, where 20 phytocompounds were identified with the abundance of ODA, NA and DMB. Based on survival and new collagen synthesis, NA was identified as the major contributing factor to the healing ability of TP. This was further confirmed by molecular assessment of candidate genes through q-PCR analysis, where all the tested genes (*nlp-29*, *itr-1* and *col-19*) were up-regulated upon treatment compared to wounded control (Fig. 6). Up-regulation of *nlp-29* is perceived to insure resistance to the pathogens by activation of anti-microbial peptides, which corroborates with the previous report by Tofoni and Pujol [44] (Fig. 10-iii). Alike, up-regulation of *itr-1*could be linked to the increase in calcium signaling, which is also in accordance with the former finding by Chisholm [45] (Fig. 10-ii). In addition, up-regulation of *col-19* infers increase in new collagen synthesis, which is also reflected in microscopic finding (Fig. 5). Overall, the q-PCR result substantiated the previous physiological assays and disclosed the major contribution of NA to the healing ability of TP. This was further validated by cell line based study (scratch wound healing assay) wherein, the results indicated that the migration rate of TP treated cells was nearly equal to that of NA treated cells and greater than that of other major phytocompounds treated cells. This result apparently divulges that the findings from *C. elegans* wound model are of high relevance to higher eukaryotic model, which can be readily compared.

Since all the experimental data infer that the healing ability of the screened extract TP was majorly contributed by NA, metabolome analysis coupled with MALDI-MS followed by molecular docking was

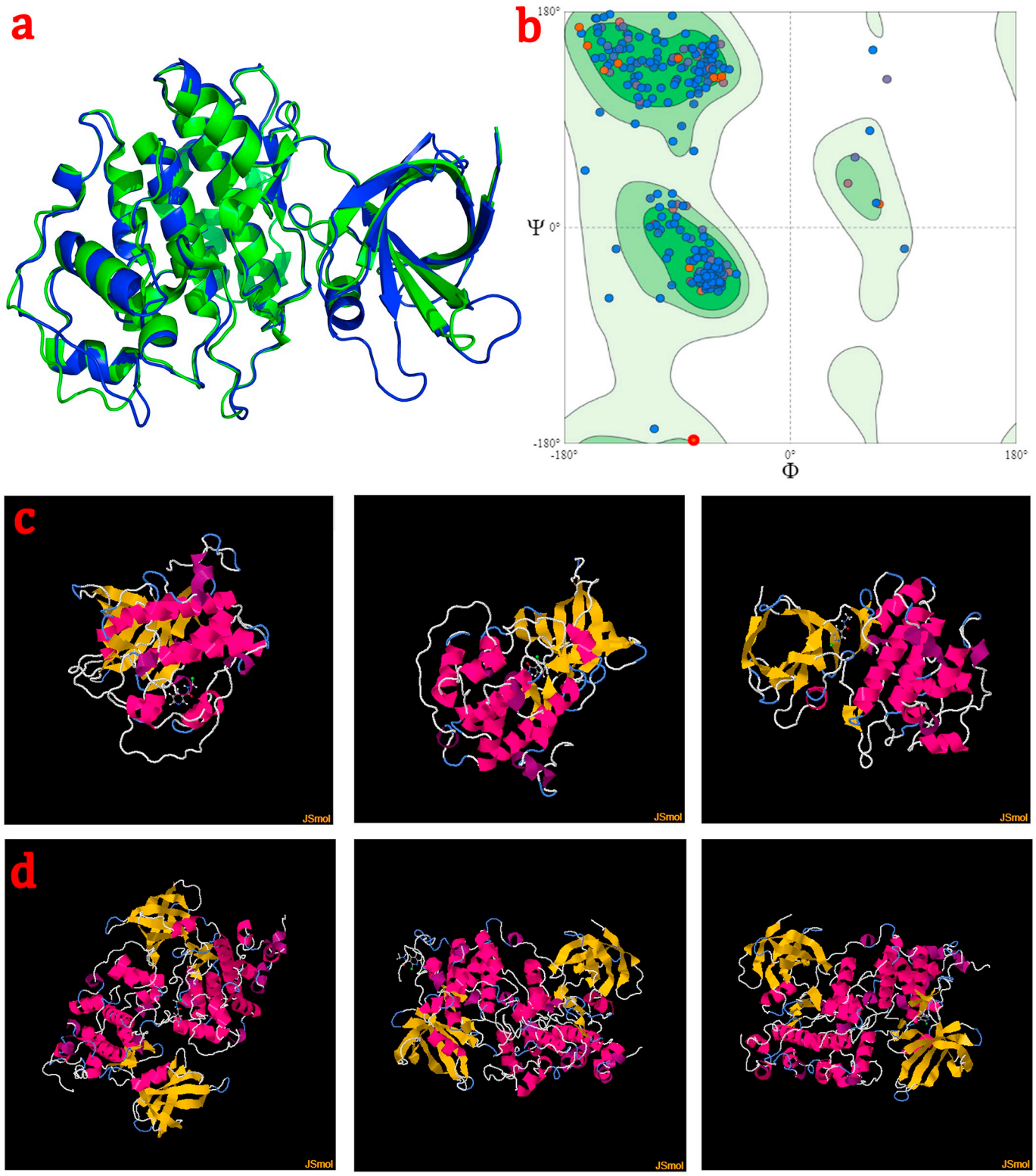

Fig. 9. Bioinformatics based evaluation of mode of action of NA (a) predicted 3d conformation of GSK-3 ortholog of human GSK-3α and β in *C. elegans* (b) confirmation of predicted structure using Ramachandran plot (c) docking results of active metabolites in its three structural variants with GSK-3 ortholog of human GSK-3α and β in *C. elegans* (d) docking results of active metabolites in its three structural variants with GSK-3 of humans. (Docking results of the ligands 3-Pyridinecarboxamide, N-(chloromethyl)-, 2-Chloro-*N*-methylnicotinamide and 6-Chloro-*N*-methylnicotinamide was given from left to right in the pictures).

performed to uncover its mode of healing. Through single worm metabolome analysis, derivative with a molecular mass of 170 was spotted to be specific for wound healing ability of NA, which was then identified to be chloromethyl nicotinamide using PubChem database. Subsequently, molecular docking of chloromethyl nicotinamide with a known wound healing biomarker, GSK-3 of *C. elegans* and humans was performed using SWISS DOCK online portal. The results revealed that the binding capacities of chloromethyl nicotinamide with GSK-3 of *C. elegans* and human origins were analogous with low binding energies. This unveils that NA exerted improved healing ability through

Table 5
Predicted binding energies of NA metabolites with GSK-3 of *C. elegans*/humans.

S. No.	Name of ligand and receptor	Estimated ΔG (kcal/mol)
1.	3-Pyridinecarboxamide, N-(chloromethyl)- with GSK-3 of *C. elegans*	−6.37
2.	2-Chloro-*N*-methylnicotinamide with GSK-3 of *C. elegans*	−6.12
3.	6-Chloro-*N*-methylnicotinamide with GSK-3 of *C. elegans*	−6.23
4.	3-Pyridinecarboxamide, N-(chloromethyl)- with GSK-3 of Humans	−6.01
5.	2-Chloro-*N*-methylnicotinamide with GSK-3 of Humans	−6.65
6.	6-Chloro-*N*-methylnicotinamide with GSK-3 of Humans	−6.57

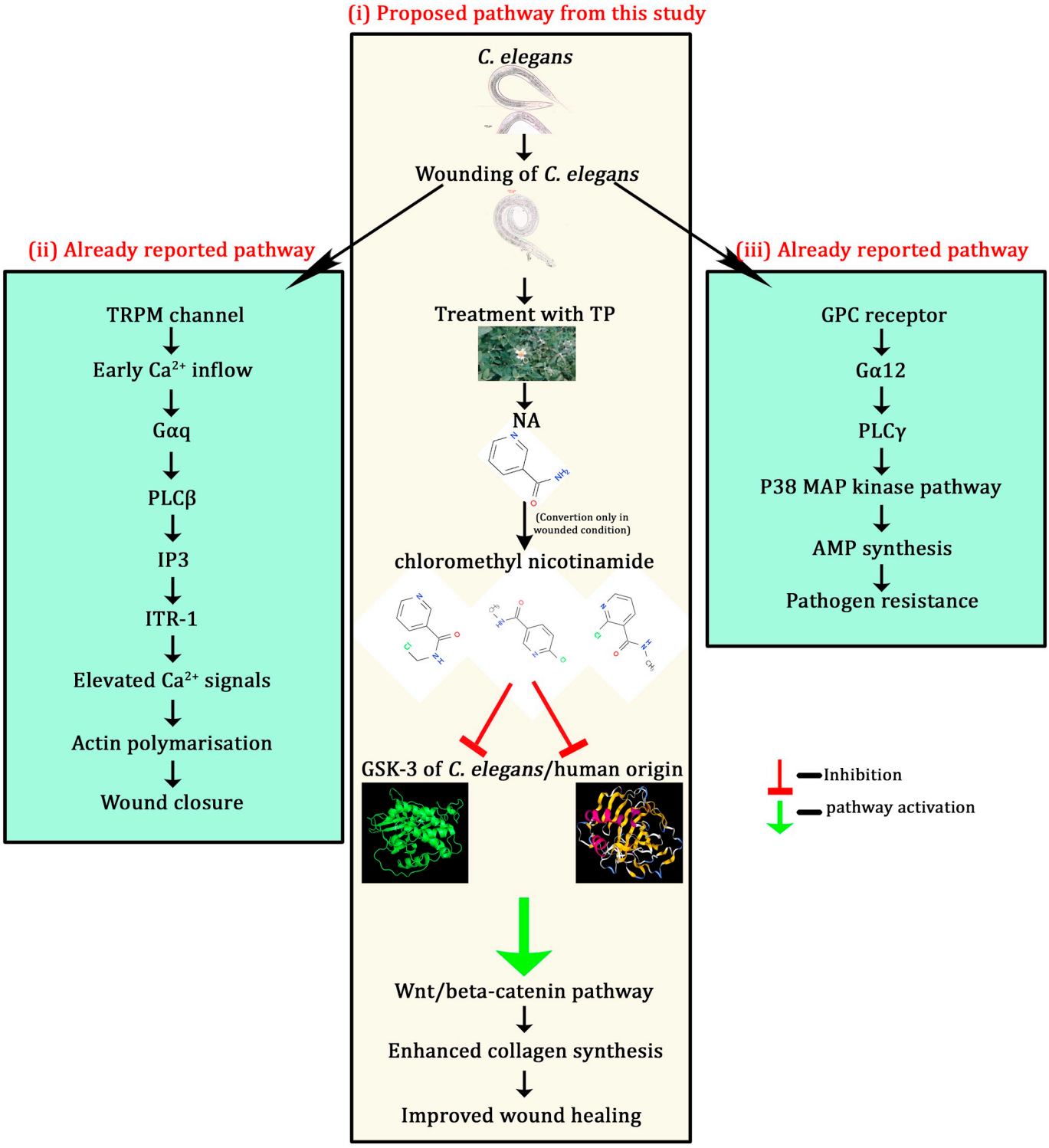

Fig. 10. Mode of healing in *C. elegans* (i) proposed mechanism of healing of NA (ii) reported mode of wound closure in *C. elegans* (iii) reported mode of pathogen resistance elucidated after injury in *C. elegans*.

inhibition ofGSK-3, which was proven to promote wound healing via activation of Wnt/β-catenin pathway [46,47]. Moreover, it was verified that the deletion of GSK-3β in a mouse model resulted in enhanced collagen synthesis and accelerated healing [48]. Hence, it is proposed in the present study that NA induces new collagen synthesis for improved healing ability through Wnt/β-catenin pathway by inhibiting GSK-3 protein in the form of chloromethyl nicotinamide only in wounded condition (Fig. 10-i). On the whole, the present study evidenced that findings from *C. elegans* wound model is comparable as well as applicable to higher eukaryotes and hence this mighty miniature model can preferentially be used as a model for preliminary high through screening of wound healing therapeutics. However, the therapeutics that are screened using *C. elegans* wound model, are required to be validated in higher models before going for human trials.

5. Conclusion

In the present study, *C. elegans* wound model was used for prescreen purpose for the first time with a new wounding protocol. This is the first study to elucidate the mode of action of identified active principle (NA) through metabolome analysis followed by molecular docking using *C. elegans* wound model. The study unveiled the specific conversion of NA to its active metabolite form only in wounded condition, chloromethyl nicotinamide which was found to confer better healing ability by inducing new collagen synthesis through inhibition of GSK-3and activation of Wnt/β-catenin pathway. Overall, the present study suggests that this elegant nematode wound model may preferentially be used as a good system for preliminary high throughput screening of active leads and aids in understanding their mode of action.

Acknowledgments and funding sources

Authors thank the *Caenorhabditis* Genetics Center, which is funded by the National Institute of Health, National Centre for Research Resources for providing the nematode strains. The Authors sincerely thank Dr. G. Kumaresan, Professor& Head, Department of Genetics, Madurai Kamaraj University for providing us with Hep3B cells. PM acknowledges the ITC India Ltd., Bangalore for the financial assistance in the form of ITC-PF. PM gratefully acknowledges the University Science Instrumentation Centre (USIC), Alagappa University. The computational facility provided by the Bioinformatics Infrastructure Facility, Alagappa University funded by the Department of Biotechnology, Ministry of Science and Technology, Government of India (Grant No. BT/BI/25/012/2012(BIF)), Instrumentation Facility provided by Department of Science and Technology (DST), Government of India through DST PURSE [Grant No. SR/S9Z-415 /2010/42(G)], DST FIST [Grant No. SR/FST/LSI-639/2015(C)], UGC through SAP-DRS1 [Grant No. F.5-1/2018/DRS-II (SAPII)] and RUSA 2.0 [Grant No. F. 24-51/2014-U, Policy (TN Multi-Gen), Dept of Edn, GOI] are thankfully acknowledged.

Declaration of competing interest

The listed authors declare no conflicts of interests.

References

[1] Y. Jiang, S. Huang, X. Fu, H. Liu, X. Ran, S. Lu, D. Hu, Q. Li, H. Zhang, Y. Li, R. Wang, Epidemiology of chronic cutaneous wounds in China, Wound Repair Regen. 19 (2) (2011) 181–188.
[2] W.H. Eaglstein, R.S. Kirsner, M.C. Robson, Food and Drug Administration (FDA) drug approval end points for chronic cutaneous ulcer studies, Wound Repair Regen. 20 (6) (2012) 793–796.
[3] R.F. Pereira, P.J. Bartolo, Traditional therapies for skin wound healing, Adv wound care. 5 (5) (2016) 208–229.
[4] M. Saxena, U.S. Patent No. 9,056,117. Washington, DC: U.S. Patent and Trademark Office, (2015).
[5] K. Hacket, C.L.B. Lowe. U.S. Patent No. 7,709,447. Washington, DC: U.S. Patent and Trademark Office 2010.
[6] L. Zhao. U.S. Patent Application No. 11/750,125 2007.
[7] A.P. Ambika, S.N. Nair, Wound healing activity of plants from the *Convolvulaceae* Family, Adv wound care. 8 (1) (2019) 28–37.
[8] R.K. Sivamani, B.R. Ma, L.N. Wehrli, E. Maverakis, Phytochemicals and naturally derived substances for wound healing, Adv wound care 1 (5) (2012) 213–217.
[9] N. Rahman, H. Rahman, M. Haris, R. Mahmood, Wound healing potentials of *Thevetia peruviana*: antioxidants and inflammatory markers criteria, J Tradi Complementary Med 7 (4) (2017) 519–525.
[10] X. Han, Y. Tao, Y. Deng, J. Yu, Y. Sun, G. Jiang, Metformin accelerates wound healing in type 2 diabetic db/db mice, Mol. Med. Rep. 16 (6) (2017) 8691–8698.
[11] Q. Shi, Z. Qian, D. Liu, J. Sun, X. Wang, H. Liu, J. Xu, X. Guo, GMSC-derived exosomes combined with a chitosan/silk hydrogel sponge accelerates wound healing in a diabetic rat skin defect model, Front. Physiol. 8 (2017) 904.
[12] F. Barré-Sinoussi, X. Montagutelli, Animal models are essential to biological research: issues and perspectives, Future Sci OA. 1 (4) (2015) FSO63.
[13] I.A. Freires, J.D.C.O. Sardi, R.D. de Castro, P.L. Rosalen, Alternative animal and non-animal models for drug discovery and development: bonus or burden? Pharm. Res. 34 (4) (2017) 681–686.
[14] S. Doke K, S. Dhawale C. Alternatives to animal testing: a review. Saudi Pharma J. 23(3) (2015) 223–229.
[15] T. Kaletta, M.O. Hengartner, Finding function in novel targets: *C. elegans* as a model organism, Nat. Rev. Drug Discov. 5 (5) (2006) 387.
[16] C.H. Lai, C.Y. Chou, L.Y. Ch'ang, C.S. Liu, W.C. Lin, Identification of novel human genes evolutionarily conserved in *Caenorhabditis elegans* by comparative proteomics, Genome Res. 10 (5) (2000) 703–713.
[17] R. Baumeister, L. Ge, The worm in us—*Caenorhabditis elegans* as a model of human disease, Trends Biotechnol. 20 (4) (2002) 147–148.
[18] M.C. Leung, P.L. Williams, A. Benedetto, C. Au, K.J. Helmcke, M. Aschner, J.N. Meyer, *Caenorhabditis elegans*: an emerging model in biomedical and environmental toxicology, Toxicol. Sci. 106 (1) (2008) 5–28.
[19] S. Xu, A.D. Chisholm, *C. elegans* epidermal wounding induces a mitochondrial ROS burst that promotes wound repair, Dev. Cell 31 (1) (2014) 48–60.
[20] S. Xu, A.D. Chisholm, A Gαq-Ca^{2+} signaling pathway promotes actin-mediated epidermal wound closure in *C. elegans*, Curr. Biol. 21 (23) (2011) 1960–1967.
[21] A. Tong, G. Lynn, V. Ngo, D. Wong, S.L. Moseley, J.J. Ewbank, A. Goncharov, Y.C. Wu, N. Pujol, A.D. Chisholm, Negative regulation of Caenorhabditis elegans epidermal damage responses by death-associated protein kinase, PNAS 106 (5) (2009) 1457–1461.
[22] M. Chuang, A.D. Chisholm, Insights into the functions of the death associated protein kinases from *C. elegans* and other invertebrates, Apoptosis 19 (2) (2014) 392–397.
[23] P. Singh, P. Ravanan, P. Talwar, Death associated protein kinase 1 (DAPK1): a regulator of apoptosis and autophagy, Front. Mol. Neurosci. 9 (2016) 46.
[24] S. Brenner, The genetics of Caenorhabditis elegans, Genetics 77 (1) (1974) 71–94.
[25] S. B. Sivamaruthi, K. Balamurugan, Physiological and immunological regulations in *Caenorhabditis elegans* infected with *Salmonella enterica* serovar Typhi, Indian J. Microbiol. 54 (1) (2014) 52–58.
[26] S. Xu, A.D. Chisholm, Methods for skin wounding and assays for wound responses in *C. elegans*, JVis Exp 94 (2014) 51959.
[27] Y. Zhang, W. Li, L. Li, Y. Li, R. Fu, Y. Zhu, J. Li, Y. Zhou, S. Xiong, H. Zhang, Structural damage in the *C. elegans* epidermis causes release of STA-2 and induction of an innate immune response, Immunity 42 (2) (2015) 309–320.
[28] S. Valentini, F. Cabreiro, D. Ackerman, M.M. Alam, M.B. Kunze, C.W. Kay, D. Gems, Manipulation of in vivo iron levels can alter resistance to oxidative stress without affecting ageing in the nematode *C. elegans*, Mech. Ageing Dev. 133 (5) (2012) 282–290.
[29] S. Sethupathy, L. Vigneshwari, A. Valliammai, K. Balamurugan, S.K. Pandian, L-Ascorbyl 2, 6-dipalmitate inhibits biofilm formation and virulence in methicillin-resistant *Staphylococcus aureus* and prevents triacylglyceride accumulation in *Caenorhabditis elegans*, RSC Adv. 7 (38) (2017) 23392–23406.
[30] S.G. Jin, A.M. Yousaf, S.W. Jang, M.W. Son, K.S. Kim, D.W. Kim, D.X. Li, J.O. Kim, C.S. Yong, H.G. Choi, In vivo wound-healing effects of novel Benzalkonium chloride-loaded hydrocolloid wound dressing, Drug Dev. Res. 76 (3) (2015) 157–165.
[31] S. Durai, N. Singh, S. Kundu, K. Balamurugan, Proteomic investigation of *Vibrio alginolyticus* challenged *Caenorhabditis elegans* revealed regulation of cellular homeostasis proteins and their role in supporting innate immune system, Proteomics 14 (15) (2014) 1820–1832.
[32] M.I. Prasanth, G.S. Santoshram, J.P. Bhaskar, K. Balamurugan, Ultraviolet-A triggers photoaging in model nematode Caenorhabditis elegans in a DAF-16 dependent pathway, Age 38 (1) (2016) 27.
[33] D.A. Mir, K. Balamurugan, A proteomic analysis of *Caenorhabditis elegans* mitochondria during bacterial infection, Mitochondrion 48 (2019) 37–50.
[34] A.D. Premarathna, T.H. Ranahewa, S.K. Wijesekera, R.R.M.K.K. Wijesundara, A.P. Jayasooriya, V. Wijewardana, R.P.V.J. Rajapakse, Wound healing properties of aqueous extracts of *Sargassum illicifolium*: an *in vitro* assay, Wound Med. 24 (1) (2019) 1–7.
[35] P. Lahiri, D. Dhaware, A. Singh, V. Panchagnula, D. Ghosh, Quantitation of neurotoxic metabolites of the kynurenine pathway by laser desorption ionization mass spectrometry (LDI-MS) in metabolomics, Methods Mol. Biol. 1996 (2019) 113–129.
[36] S.M. Vidya, V. Krishna, B.K. Manjunatha, B.R. Bharath, K.P. Rajesh, H. Manjunatha, K.L. Mankani, Wound healing phytoconstituents from seed kernel of *Entada pursaetha* DC. and their molecular docking studies with glycogen synthase kinase 3-β, Med. Chem. Res. 21 (10) (2012) 3195–3203.
[37] A. Grosdidier, V. Zoete, O. Michielin, SwissDock, a protein-small molecule docking web service based on EADock DSS, Nucleic Acids Res. 39 (2011) 270–277.
[38] A.D. Chisholm, T.I. Hsiao, The *Caenorhabditis elegans* epidermis as a model skin. I: development, patterning, and growth, Wiley Interdiscip. Rev. Dev. Biol. 1 (6) (2012) 861–878.
[39] N. Pujol, S. Cypowyj, K. Ziegler, A. Millet, A. Astrain, A. Goncharov, Y. Jin,

A.D. Chisholm, J.J. Ewbank, Distinct innate immune responses to infection and wounding in the *C. elegans* epidermis, Curr. Biol. 18 (7) (2008) 481–489.
[40] R. Van der Hoeven, K.C. McCallum, D.A. Garsin, Speculations on the activation of ROS generation in *C. elegans* innate immune signaling, Worm 1 (3) (2012) 160–163.
[41] W. Wood, Wound healing: calcium flashes illuminate early events, Curr. Biol. 22 (1) (2012) 14–16.
[42] N.H. Tang, A.D. Chisholm, Regulation of microtubule dynamics in axon regeneration: insights from *C. elegans*, F1000Res. 5 (2016) 764.
[43] M. Xue, C.J. Jackson, Extracellular matrix reorganization during wound healing and its impact on abnormal scarring, Adv Wound Care 4 (3) (2015) 119–136.
[44] C. Taffoni, N. Pujol, Mechanisms of innate immunity in *C. elegans* epidermis, Tissue Barriers 3 (4) (2015) e1078432.
[45] A. D Chisholm. Epidermal wound healing in the nematode *Caenorhabditis elegans*. Advances in wound care. 4 (4) (2015)264–71.
[46] B.G. Harish, V. Krishna, H.S. Kumar, B.K. Ahamed, R. Sharath, H.K. Swamy, Wound healing activity and docking of glycogen-synthase-kinase-3-β-protein with isolated triterpenoid lupeol in rats, Phytomedicine 15 (9) (2008) 763–767.
[47] H. Raja Naika, V. Krishna, K. Lingaraju, V. Chandramohan, M. Dammalli, P.N. Navya, D. Suresh, Molecular docking and dynamic studies of bioactive compounds from *Naravelia zeylanica* (L.) DC against glycogen synthase kinase-3β protein, J Taibah Univ Sci 9 (1) (2015) 41–49.
[48] M. Kapoor, S. Liu, X. Shi-Wen, K. Huh, M. McCann, C.P. Denton, J.R. Woodgett, D.J. Abraham, A. Leask, GSK-3β in mouse fibroblasts controls wound healing and fibrosis through an endothelin-1–dependent mechanism, J. Clin. Invest. 118 (10) (2008) 3279–3290.